ISSN 1001-0742
CN 11-2629/X

JES

JOURNAL OF ENVIRONMENTAL SCIENCES

March 1, 2015 Volume 29
www.jesc.ac.cn

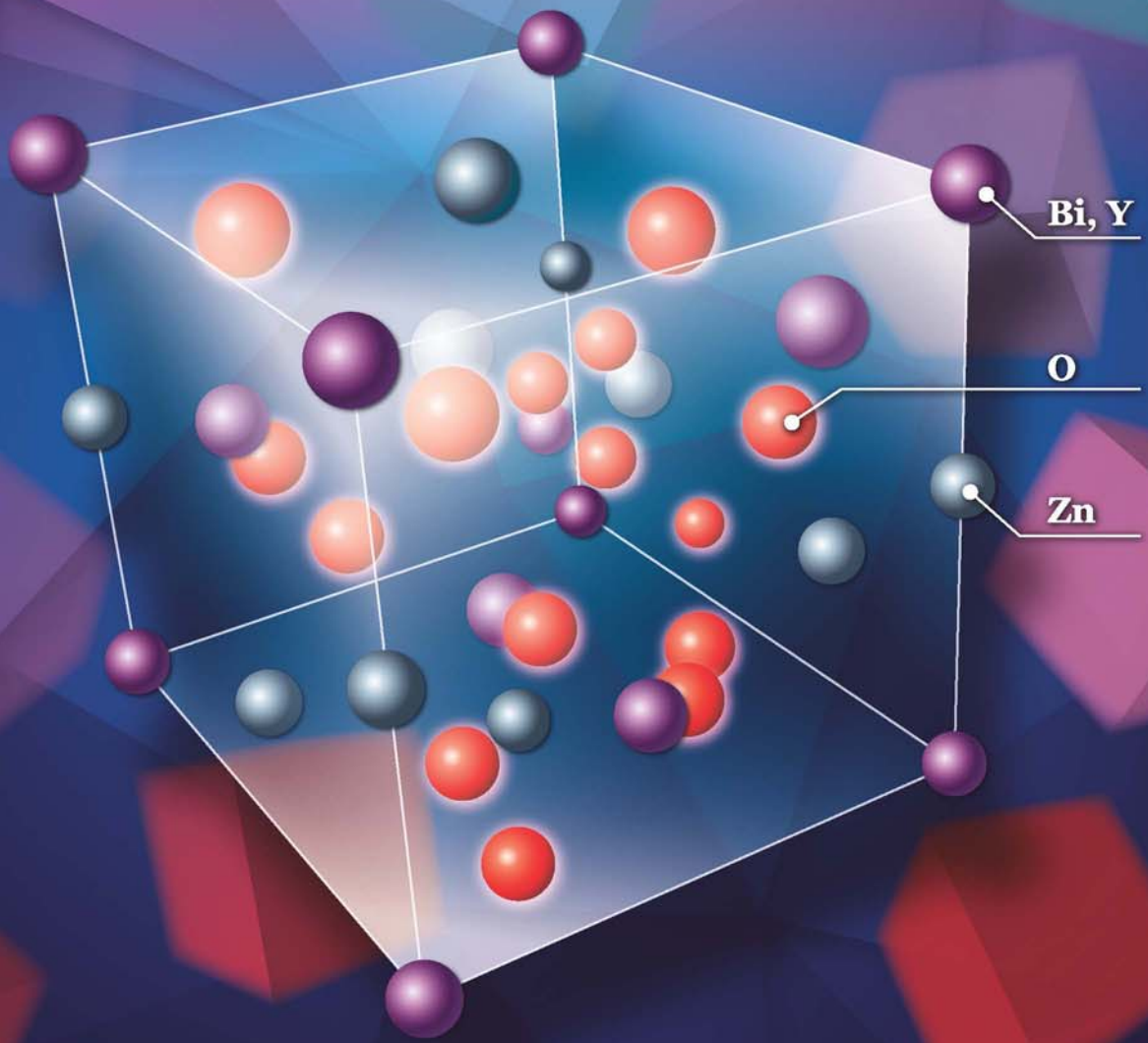

ELSEVIER
Science Press

Sponsored by
Research Center for Eco-Environmental Sciences
Chinese Academy of Sciences

Journal of Environmental Sciences Volume 29 2015

www.jesc.ac.cn

(continued on inside back cover)

CONTENTS

Available online at www.sciencedirect.com

ScienceDirect

www.journals.elsevier.com/journal-of-environmental-sciences

JOURNAL OF ENVIRONMENTAL SCIENCES
www.jesc.ac.cn

Enhanced catalytic complete oxidation of 1,2-dichloroethane over mesoporous transition metal-doped γ-Al_2O_3

Abbas Khaleel, Muhammad Nawaz*

Department of Chemistry, United Arab Emirates University, P.O. Box 17551, Al-Ain, Abu Dhabi, United Arab Emirates.
E-mail: abbask@uaeu.ac.ae

ARTICLE INFO

Article history:
Received 28 April 2014
Revised 29 September 2014
Accepted 11 October 2014
Available online 3 February 2015

Keywords:
Chlorinated organic compounds
Catalytic oxidation
Sol–gel method
Mixed metal oxides

ABSTRACT

High-surface-area mesoprous powders of γ-Al_2O_3 doped with Cu^{2+}, Cr^{3+}, and V^{3+} ions were prepared *via* a modified sol–gel method and were investigated as catalysts for the oxidation of chlorinated organic compounds. The composites retained high surface areas and pore volumes comparable with those of undoped γ-Al_2O_3 and the presence of the transition metal ions enhanced their surface acidic properties. The catalytic activity of the prepared catalysts in the oxidation of 1,2-dichloroethane (DCE) was studied in the temperature range of 250–400°C. The catalytic activity and product selectivity were strongly dependent on the presence and the type of dopant ion. While Cu^{2+}- and Cr^{3+}-containing catalysts showed 100% conversion at 300°C and 350°C, V^{3+}-containing catalyst showed considerably lower conversion. Furthermore, while the major products of the reactions over γ-alumina were vinyl chloride (C_2H_3Cl) and hydrogen chloride (HCl) at all temperatures, Cu- and Cr-doped catalysts showed significantly stronger capability for deep oxidation to CO_2.

Introduction

Chlorinated organic compounds are considered as major contributors to air pollution due to their toxicity and their contribution to ozone depletion. Catalysts based on noble metal particles as well as metal oxides have been widely studied for the oxidative degradation of chlorinated hydrocarbons as a promising method for their emission control and removal. While supported noble metal catalysts exhibit, generally, higher catalytic activities as compared with metal oxide catalysts, they have some disadvantages including: (a) their higher costs, (b) deactivation due to their sensitivity to poisons, and (c) sintering at higher temperatures (Scire et al., 2003). On the other hand, transition metal oxide catalysts have several advantages including acid–base and redox properties, higher thermal stability, lower costs, and the possibility of fabrication in high surface area porous powders. Therefore, transition metal oxides have been studied extensively as appropriate catalysts for the total combustion of chlorinated hydrocarbons (Khaleel and Al-Nayli, 2008; Aranzabal et al., 2006). Among the catalytic systems that have shown promising performance are vanadium oxide-based materials (Larrubia and Busca, 2002), $AMnO_3$ perovskites (A represents lanthanide ions) (Zhang et al., 2013), Cr_2O_3, and Fe_2O_3-based catalysts (Khaleel and Al-Nayli, 2008; López-Fonseca et al., 2000).

The catalytic oxidation of 1,2-dichloroethane (DCE), as a typical chlorinated organic pollutant, has been reported to take place on several catalysts including metal particles, metal oxides, and zeolites-based catalysts (de Rivas et al., 2013; Aranzabal et al., 2006; Huang et al., 2010). In most of the reported studies, it was found that DCE first decomposed to vinyl chloride (C_2H_3Cl), and HCl followed by oxidation to CO and CO_2. However, deep oxidation took place at relatively high temperatures, around 400°C, and the selectivity was very low. In previous studies we found that γ-alumina-based catalysts exhibited promising activity towards the adsorption and decomposition of some chlorinated hydrocarbons (Khaleel and Dellinger, 2002; Khaleel, 2006). We also found that catalysts based on bulk mixed oxides can exhibit significantly enhanced catalytic activity in these reactions compared with their

* *Corresponding author.*

http://dx.doi.org/10.1016/j.jes.2014.09.032

corresponding single metal oxides as well as their supported counterparts (Khaleel and Al-Nayli, 2008).

The main objective of the present work was to combine the well-known ability of γ-alumina surface to promote dehydrochlorination with the redox properties of transition metal ions in order to enhance the deep oxidation of chlorinated organic compounds. The effect of doping γ-alumina with Cu^{2+}, Cr^{3+}, and V^{3+} on its catalytic activity in the oxidation of DCE was studied.

1. Experimental

1.1. Catalysts preparation

Chemicals including aluminum *sec*-butoxide (ASB), $Cr(NO_3)_3{\cdot}9H_2O$, 2-propanol, methanol, copper(II) acetylacetonate (Cu(II) acac), and VCl_3 of purity >97% were purchased from Aldrich and were used without further purification. Doubly distilled water was used in the hydrolysis reactions.

Powders of γ-Al_2O_3 doped with Cu^{2+}, V^{3+}, and Cr^{3+} were prepared *via* a sol–gel method. The general formula Al-M-x will be used to represent the doped catalysts where "M" refers to the dopant metal ion and "x" refers to its molar fraction, 100 × M/M + Al. Composites with 3% Cu^{2+}, V^{3+}, and Cr^{3+} as well as composites with 5% and 10% Cu^{2+} were prepared. ASB and Cr(III) nitrate precursors were dissolved in 2-propanol and V(III) chloride and Cu(II) acac were dissolved in methanol. In a typical experiment on the preparation of Al–Cr-3, as an example, 6 mL (0.023 mol) of ASB was dissolved in 200 mL 2-propanol and the desired amount of chromium nitrate was dissolved in 50 mL 2-propanol separately. The Cr^{3+} solution was added to the ASB solution and the mixture was stirred for 20 min. While stirring, 2.0 mL (0.11 mol) water was added dropwise to the mixture which was stirred more for 4 hr and aged for 16 hr in a covered beaker. The solvent was then evaporated at around 80°C and the obtained powders were dried in an oven at 120°C for 1 hr before calcination at 500°C for 5 hr. Undoped γ-Al_2O_3 was prepared *via* the same procedure.

1.2. Material characterization

Powder X-ray diffraction (XRD) patterns were obtained using a Philips (USA) PW/1840 diffractometer (40 kV, 25 mA) with Cu-Kα radiation, λ = 1.542 Å. Data was collected in the 2θ angle range of 20–80° at a rate of 2°/min.

Diffuse reflectance infrared Fourier transform spectra (DRIFTS) were collected in the 400–4000 cm^{-1} range at 4 cm^{-1} resolution using a Shimadzu (Japan) IR-Affinity-1 spectrometer. The DRIFTS accessory, from Pikes Technologies, was equipped with a heated cell for *in-situ* studies with the capability of heating to temperatures as high as 900°C. The samples were prepared in potassium bromide (KBr) powder mixtures, 10% by mass. A background spectrum was recorded for KBr at 25°C after pretreatment at 150°C under nitrogen flow, 10 mL/min. The samples were then heated under the same N_2 flow to 400°C at a rate of 10°/min and were soaked for 20 min before spectra were recorded.

N_2 adsorption studies at 77 K for surface area and porosity measurements were conducted on an Autosorb-1 (Quantochrome, USA) volumetric gas sorption instrument. Samples were degassed at 150°C for 1 hr before measurements. The surface area was obtained by the Brunauer–Emmett–Teller (BET) method and the pore size distributions were determined by Barett–Joyner–Halenda (BJH) model from the desorption branch of the N_2 isotherms.

Pyridine adsorption was studied using DRIFTS and spectra were collected in the 400–4000 cm^{-1} range at 4 cm^{-1} resolution using a Shimadzu IR-Affinity-1 spectrometer. Powder samples, *ca*. 200 mg, were pretreated under N_2 flow, 10 mL/min at 400°C for 1 hr then cooled down to 120°C for pyridine adsorption. Pyridine was introduced by switching the N_2 flow through a pyridine saturator at room temperature for 20 min. The temperature was then raised to 150°C and the sample chamber was purged with N_2 gas for 20 min to remove free pyridine vapor. Several IR spectra were then collected at the same temperature, 150°C. A background spectrum of the powder, recorded for the sample after heat treatment at 150°C before introducing pyridine, was subtracted from each spectrum.

Temperature programmed desorption (TPD) of NH_3 was performed on a ChemBET TPR/TPD chemisorption analyzer from Quantachrome equipped with a thermal conductivity detector (TCD). Prior to adsorption, the samples (200 mg) were pretreated in a quartz U-tube at 300°C for I hr under helium (He) flow. The samples were then cooled down to 120°C under He stream, 30 mL/min, and were soaked at this temperature for 20 min. The adsorption of NH_3 was performed by saturating the samples with NH_3 using 20 mL/min flow for 30 min at the same temperature. The samples were then purged with He (30 mL/min) for 30 min to remove reversibly and physically bound ammonia from the surface. Desorption was carried out from 120°C to 600°C at a heating rate of 20°C/min.

Temperature programed reduction (TPR) experiments were carried out on the same instrument described above for TPD study. In each experiment, 100 mg sample was placed in a U-shaped Pyrex tube and prior to reduction, the sample was degassed at 300°C for 30 min in N_2 at a flow rate of 30 mL/min. After cooling to 100°C, the sample was heated to 875°C at a rate of 30°C/min under the flow of the reducing gas mixture, 5% H_2 diluted in N_2, at a flow rate of 50 mL/min. The H_2 uptake during the reduction was measured by a TCD.

1.3. Catalytic activity study

The catalytic activity was investigated using a fixed-bed flow reactor under atmospheric pressure. The reactor was coupled in-line with a continuous flow FT-IR gas cell, from Pikes Technology, for continuous monitoring of the reaction products. The reactor was made of U-shape stainless steel tube heated by a tube furnace equipped with a temperature controller and a K-type thermocouple. The reaction feed, monitored by mass flow controllers, was composed of O_2/N_2 mixture (20% O_2) at a flow rate of 20 mL/min and DCE vapor introduced to the feed by a syringe pump at a rate of 2.5 μL/min. The injection point was electrically heated to ensure immediate evaporation of DCE in the feed stream which was allowed to mix well before entering the reactor. The catalyst (125 mg, 180–355 mesh) was packed in the reactor between a stainless steel frit and a glass wool plug. Before each reaction, the catalyst was pretreated at 400°C for 1 hr under O_2/N_2 flow. After maintaining the desired reaction temperature, DCE was introduced and the eluting products were allowed to flow

continuously through the heated gas cell. The transfer line and the IR cell were heated at 150°C to prevent any condensation. FT-IR spectra of the products were recorded every 5 min during the first 30 min and then every 1 hr for the rest of the time on stream, a total of 5 or 36 hr in selected experiments. Ten spectra were recorded continuously each time within a period of 2 min. The spectrum of the cell, recorded prior to each reaction with O_2/N_2 flow, was subtracted as a background.

The conversion of DCE was determined from the integration of its characteristic peak for ρCH_2 at 1238 cm^{-1} using a calibration curve, linear coefficient of 0.99, based on a series of blank experiments, in the absence of a catalyst, where different DCE concentrations were used under the same experimental conditions. Since a quantitative study of the different products and intermediates was difficult using the employed FT-IR method alone, the present study is concerned mainly with the selectivity to the main products, CO_2 and C_2H_3Cl, in order to compare the ability of the different catalysts to deeply oxidize DCE. The CO_2 and C_2H_3Cl (VC) selectivity was evaluated by scaling their FT-IR characteristic peak intensities *via* peak integration using the same peaks in the spectra of reactions over γ-Al_2O_3 as a reference. The characteristic peaks used to evaluate CO_2 and C_2H_3Cl are those at 2358 and 1610 cm^{-1}, respectively. Conversion measurements and product profiles were considered at steady state, which was usually achieved after 20 min on stream.

1.4. DCE adsorption

DCE adsorption and subsequent decomposition on the surface of the catalysts was studied *in-situ* using DRIFTS. Spectra were recorded in the 400–4000 cm^{-1} range at 4 cm^{-1} resolution using a Shimadzu IR-Affinity-1 spectrometer and DRIFTS accessory equipped with a cell for *in-situ* studies under variable temperatures. In a typical experiment, ~200 mg of the catalyst, placed in a ceramic cup, was pretreated at 500°C under dry air flow, 20 mL/min, for 1 h. The sample was then cooled down to 100°C and the air flow was replaced by N_2 before a background spectrum was recorded. DCE was introduced by passing the N_2 flow through a DCE saturator at room temperature. After 20 min, a spectrum was recorded before the cell was purged with N_2 gas for 30 min. After purging, a spectrum of the catalyst was recorded at the same temperature, 100°C. The catalyst was then heated to 200°C and was soaked at this temperature for 20 min followed by cooling to the same temperature of the background spectrum, 100°C, before a spectrum was recorded again. The last step was repeated for spectra at 300°C and 400°C.

2. Results and discussion

2.1. Catalysts characterization

The employed sol–gel method resulted in amorphous or very weakly crystalline powders as indicated by their XRD patterns. They showed no reflections or weak and broad reflection peaks that represent γ-alumina as shown in Fig. 1. The absence of peaks for segregated oxides of the dopant ions and the enhanced amorphous nature of the doped catalysts compared with undoped γ-alumina indicate that the dopant ions were well dispersed in the alumina matrix and played a role in hindering crystallization.

DRIFT spectra of γ-Al_2O_3, V_2O_3, and Al–V-3, are presented in Fig. 2 and similar features were observed for Al–Cu and Al–Cr composites which were presented in a previous publication (Khaleel et al.,, 2013). Fig. 2 presents the region of the spectra where characteristic absorptions due to metal–oxygen vibrations are located. γ-Alumina has a defect spinel structure with either cubic unit cell, as most spinel compounds, or a tetragonally distorted unit cell. The cubic γ-alumina is expected to exhibit 4 IR-active vibrational modes while the tetragonal one is expected to exhibit 10 active vibrational modes (Gutiérrez-Alejandre et al., 1998) making the features in their spectra difficult to assign especially if a mixture of both structures is present. The spectrum of Al–V-3 showed new peaks as well as changes in the position of other major peaks compared with those of γ-alumina. The new features include a significant decrease in the intensity of the alumina peak at ~507 cm^{-1} and the appearance of a new peak at 498 cm^{-1}. These differences indicate noticeable changes in the vibrational modes of the bulk and the surface, which represents changes in the metal–oxygen bonding confirming the incorporation of V^{3+} ions in the γ-Al_2O_3 matrix. The characteristic peaks of vanadium oxide around 630 and 485 cm^{-1} were not present in the spectrum of the composite indicating the absence of segregated vanadium oxide.

The N_2 adsorption study showed that the undoped and doped catalysts were composed of mesoporous powders of relatively high surface areas and pore volumes. In a recent study, we found that the absence of an acid gelation catalyst resulted in high surface areas and large total pore volumes (Khaleel and Al-Mansouri, 2010; Khaleel et al.,, 2013), and therefore the same conditions were employed in the present work. Table 1 presents selected textural properties of the catalysts after calcinations at 500°C. It was noticed that the

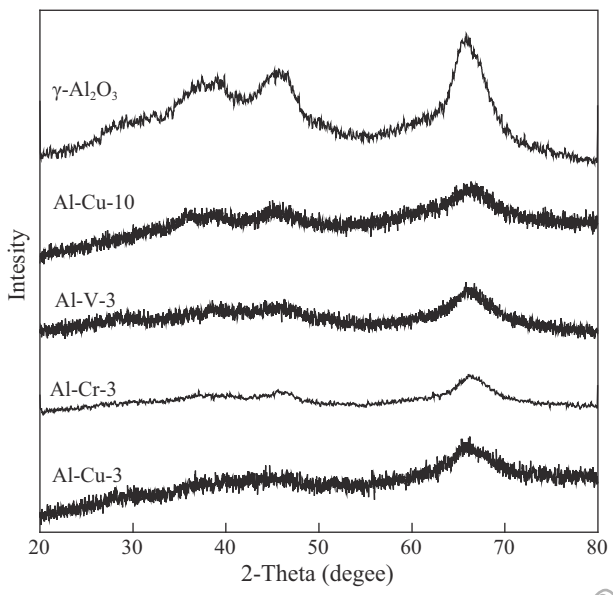

Fig. 1 – Powder XRD patterns of the prepared catalysts.

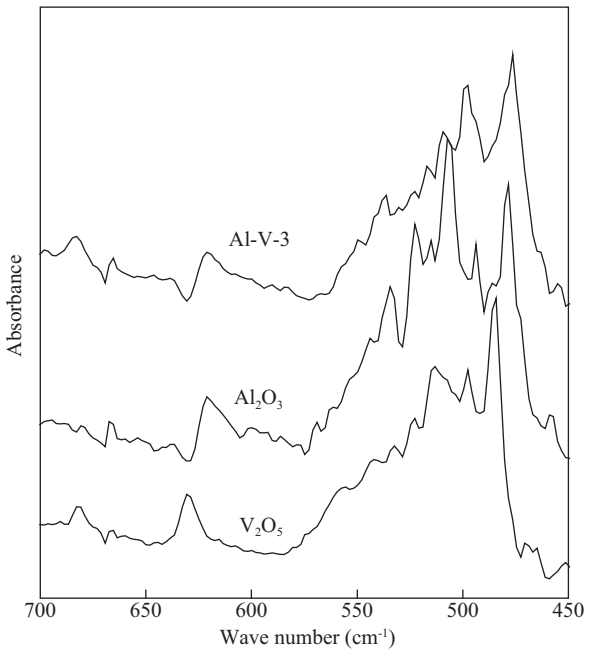

Fig. 2 – DRIFT spectra of Al_2O_3, V_2O_5, and Al–V-3 pretreated at 400°C.

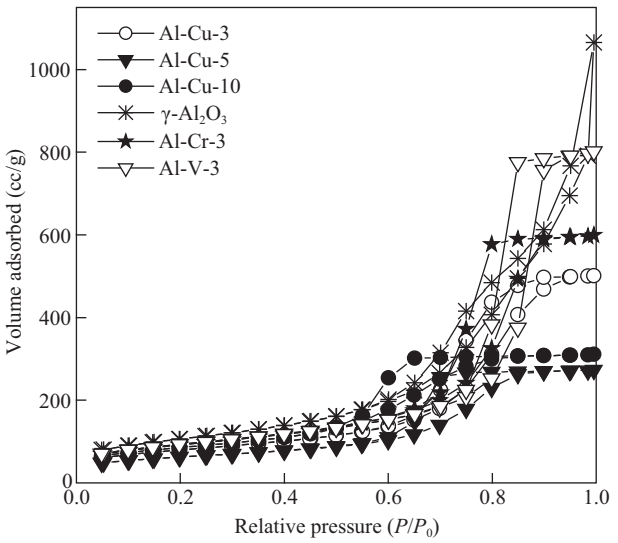

Fig. 3 – N_2 adsorption–desorption isotherms of the calcined catalysts.

presence of the dopant ions resulted, generally, in a decrease in the surface area and pore volume depending on the nature of the dopant ion and its concentration. However, all doped catalysts retained relatively high surface areas and pore volumes and homogeneous pore size distribution. It was also noticed that the composite with high Cu^{2+} content, Al–Cu-10, showed a surface area higher than those of the other Cu-containing samples. This may be referred to the enhanced incorporation of Cu^{2+} ions in the alumina lattice resulting in enhanced lattice distortion, which hinders the crystal growth process leading to smaller crystallites. Figs. 3 and 4 present the N_2 adsorption–desorption isotherms and the pore size distribution of the catalysts. All catalysts showed type-IV isotherms, Fig. 3, with hysteresis loops in the relative pressure, P/P_o, range of 0.65–0.85, which indicates the formation of mesoporous powders. The plateau in the isotherms of the doped catalysts at high relative pressures, > 0.85, indicates the absence of large-range mesopores and macropores, which were observed in the undoped γ-alumina. The BJH pore size distributions (Fig. 4) showed relatively homogeneous mesopores in all doped catalysts with diameters in the range of 5–15 nm. In spite of the observed decrease in the surface areas and pore volumes of the doped catalysts, compared with the undoped γ-alumina, the Cu^{2+}- and Cr^{3+}-containing catalysts exhibited enhanced catalytic activity as discussed in the next section.

The pyridine adsorption study showed that the presence of metal ions in the alumina matrix resulted in noticeable changes in the pyridine adoption modes, and hence in the nature of acid sites, which were dependent on the type and concentration of the dopant ion. Fig. 5 shows the infrared spectra, 1400–1700 cm^{-1} region, of pyridine adsorbed on the surface of Al–M-3 catalysts at 150°C. The spectrum of adsorbed pyridine on γ-alumina showed peaks that represent pyridine adsorbed on Lewis acid sites, 1612 and 1446 cm^{-1}, as well as peaks for pyridine bound to Brønsted acid sites, 1552

Table 1 – BET surface area and pore characteristics for doped and pure γ-Al_2O_3.

Compositions	S_{BET} (m^2/g)	Pore volume (cc/g)	Pore size (nm)
γ-Al_2O_3	367	1.32	14.4
Al-Cu-3	274	0.75	10.2
Al-Cu-5	217	0.42	7.8
Al-Cu-10	301	0.48	6.5
Al-Cr-3	327	0.66	8.1
Al-V-3	287	0.63	10.7

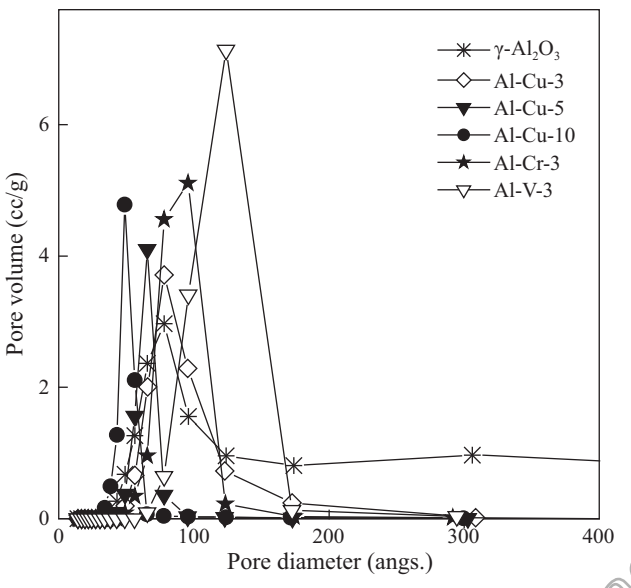

Fig. 4 – BJH pore size distributions of the calcined catalysts.

and 1493 cm^{-1} (Chakraborty and Viswanathan, 1999). The peak representing adsorption on Brønsted acid sites, at 1552 cm^{-1}, disappeared from the spectra of doped catalysts. On the other hand, more intense peaks for adsorption on Lewis acid sites were observed for Al–Cr-3 and Al–V-3, while peaks in the spectrum of Al–Cu-3 are noticeably weaker indicating lower tendency to pyridine adsorption. Another noteworthy observation was the presence of weak peaks in the spectrum of Al–Cu-3 at 1505, 1520, 1540, and 1558 cm^{-1} which were not present in the spectra of the other catalysts. These peaks more likely represent adsorption modes of pyridine on different Brønsted acid sites. Also noteworthy was the peak at 1595 cm^{-1} and the enhanced absorption at 1445 cm^{-1} in the spectrum of Al–V-3, which can be attributed to hydrogen bonded pyridine adsorbed on Lewis acid sites (Lif et al., 2007).

The NH_3 TPD results showed that the number of acid sites in Al–M-3 catalysts were higher than that in undoped γ-alumina as shown in Table 2. Concerning the strength of the acid sites, which is usually related to the desorption temperature, all catalysts showed relatively strong acid sites as indicated by desorption curves in a high temperature range between 300°C and 525°C as shown in Fig. 6. The desorption curves are relatively broad indicating a wide range of acid strength with a maximum desorption temperature between 350°C and 400°C.

The H_2-TPR profiles showed different reduction behaviors for the different catalysts as shown in Fig. 7 and Table 3. The profiles of the catalysts with 3% of different metal ions indicate that Al–Cu-3 and Al–Cr-3 exhibited stronger reducibility compared with Al–V-3, which showed less H_2 consumption and a reduction peak at a considerably higher temperature. This behavior of Al–V-3 is what one would expect as vanadium is more stable in its higher oxidation sates, and V(III) is a low oxidation state of vanadium. On the other hand, lower oxidation states of chromium and copper

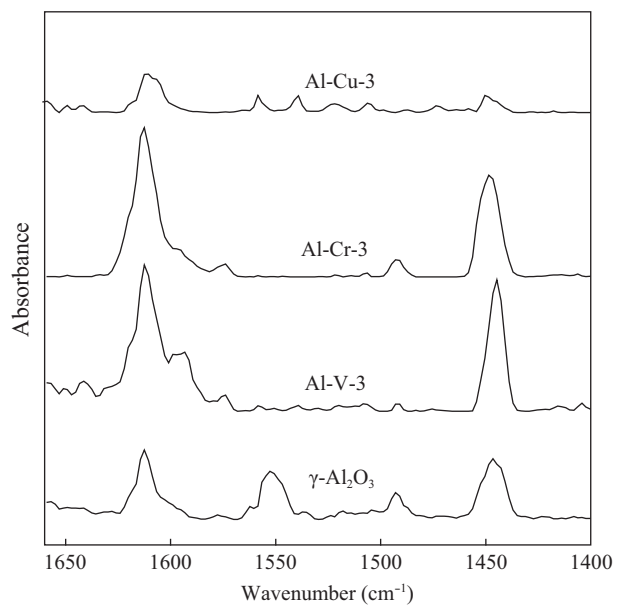

Fig. 5 – DRIFT spectra of pyridine adsorbed on Al–M-3 and γ-Al_2O_3 at 150°C.

Table 2 – NH_3 TPD results.

Catalysts	(μmol·NH_3/g)	(μmol·NH_3/m^2)
γ-Al_2O_3	273	0.74
Al–V-3	460	1.60
Al–Cr-3	602	1.84
Al–Cu-3	384	1.40
Al–Cu-5	414	1.91
Al–Cu-10	297	0.97

are more accessible due to stronger *d*-orbital radial penetration and higher effective nuclear charge which stabilize low oxidation states. The two peaks observed in the Al–Cu-3 profile most likely refer to stepwise reduction of Cu^{2+} to Cu^{1+} and Cu^0. The catalysts with higher Cu^{2+} loadings showed different reduction profiles with larger H_2 consumption due to higher Cu^{2+} concentration. While Al–Cu-5 showed a profile with two distinguished peaks similar to Al–Cu-3, Al–Cu-10 showed a very broad peak that can be due to the higher Cu^{2+} content and possible different modes of interaction with the alumina lattice. More importantly, as the Cu^{2+} concentration increased, the major reduction peak shifted to lower temperatures as shown in Fig. 7. This behavior can be referred to the increasing amount of Cu^{2+} close to the surface which is more accessible than the bulk ions.

2.2. Catalytic activity

The doped γ-alumina catalysts showed interesting results where a promising catalytic activity for the complete oxidation of DCE was enhanced by the presence of certain dopant

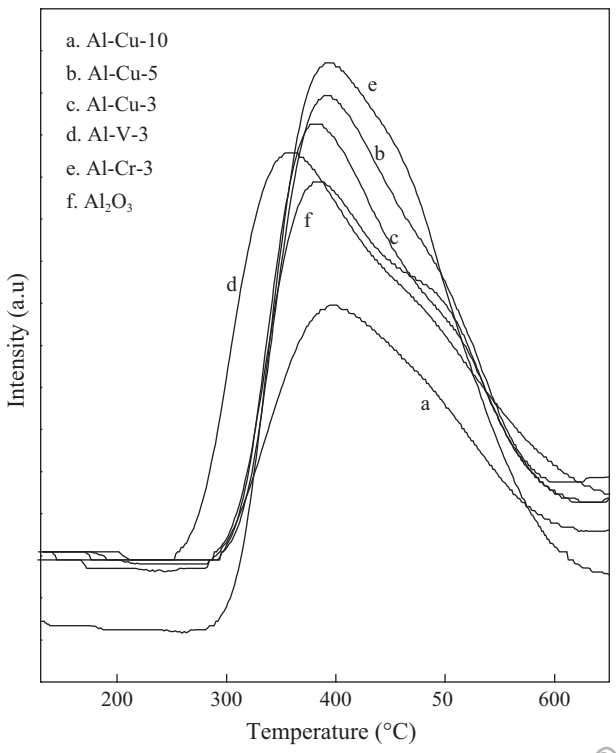

Fig. 6 – Ammonia TPD profiles for the different catalysts.

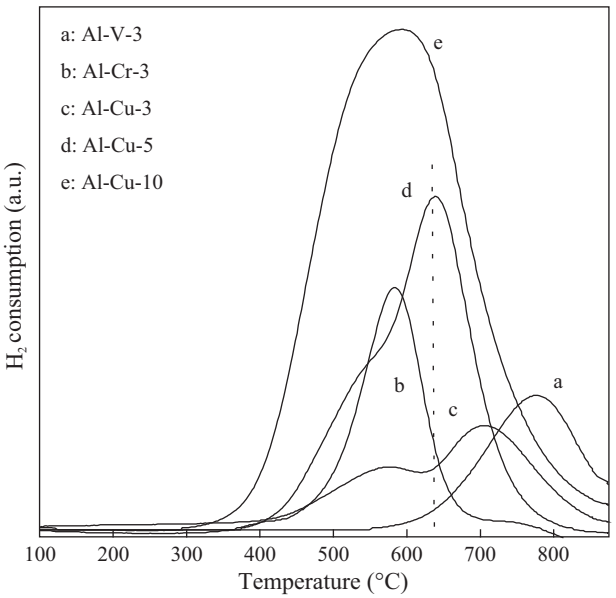

Fig. 7 – H_2-TPR profiles of the catalysts after calcination at 500°C.

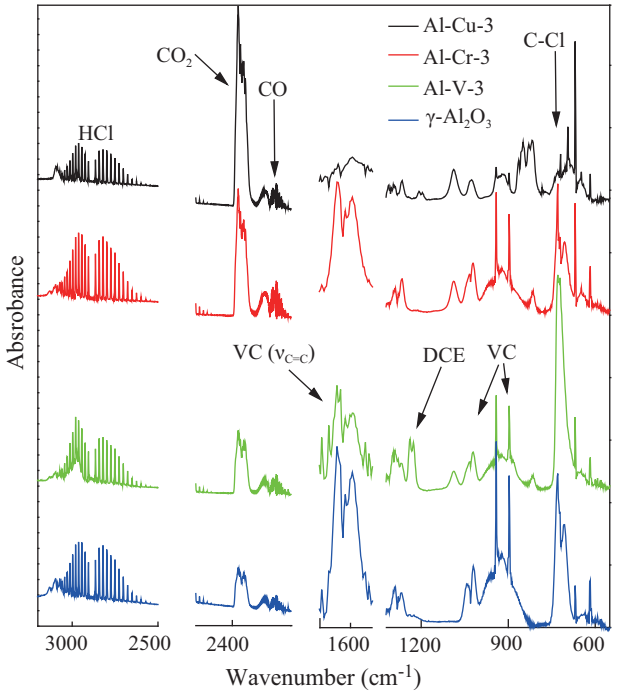

Fig. 8 – Representative FTIR spectra of the products of reactions after 5 hr on stream over undoped γ-alumina and doped γ-alumina containing 3% dopant ions.

ions. The products as identified by FT-IR spectroscopy included mainly vinyl chloride (VC), identified by its $\nu_{C=C}$ IR absorption at 1610 cm^{-1}, CO_2, HCl, and some CO. Representative FT-IR spectra of the products after 5 hr on stream over Al–M-3 catalysts at 350°C are shown in Fig. 8. Reactions over undoped γ-alumina produced VC and HCl as major products and relatively small amounts of CO_2. However, reactions over Cu- and Cr-doped catalysts showed enhanced capability for deep oxidation forming significantly larger amounts of CO_2. The spectra from reactions over Al–Cu-3 catalyst showed, in addition to the main products, new peaks in the region of 815–940 cm^{-1}, which very likely refer to some C_2HCl_3 and C_2Cl_4 byproducts based on comparison with their standard spectra. While these byproducts can be confirmed using other methods, in the rest of this study we will focus on comparing the conversion over the different catalysts and their ability to completely oxidize DCE to CO_2.

The total conversion of DCE was dependent on the type of the dopant ion used as shown in Fig. 9a. While the presence of Cr^{3+} and Cu^{2+} enhanced the conversion, compared to pure γ-alumina, V^{3+} resulted in a considerable decrease in the conversion at both studied temperatures, 300°C and 350°C. The catalytic activity of the Cu-doped catalyst was also tested in 36 hr reactions, not shown, where the conversion was very consistent during the time on stream. Not only the total conversion, but also the nature of the products showed a strong dependence on the type of dopant. While VC was the major Cl-containing hydrocarbon product from reactions over Al–V-3 and Al–Cr-3, it formed only in negligible amounts over Al–Cu-3 catalyst, Figs. 8 and 9b. More importantly, the deep oxidation to CO_2 was significantly enhanced by Al–Cu-3 resulting in significantly larger amount of CO_2 and less amount of VC.

Table 3 – Summary of the H_2-TPR results.

Catalyst	Temperature		H_2 consumption (μmol/g)		
	Peak 1	Peak 2	Peak 1	Peak 2	Total
Al–V-3	–	767	–	180.2	108.2
Al–Cr-3	599	750	180.5	26.7	207.2
Al–Cu-3	528	700	17.8	162.8	180.6
Al–Cu-5	505	633	59.6	324.5	384.1
Al–Cu-10	486	580	40.6	756.6	797.2

The catalytic activity of Cu-doped catalysts was also studied *versus* Cu^{2+} concentration. Fig. 10a presents the total conversion of DCE over catalysts with different Cu^{2+} concentrations *vs.* time on stream at 350°C. The total conversion decreased as the Cu^{2+} concentration increased especially over Al–Cu-10. This may be referred to the observed decrease in acid sites concentration, Table 2, which could be due to possible larger amount of Cu^{2+} ions on the surface replacing the acidic Al^{3+} sites. However, the decrease in conversion was very small over Al–Cu-5 where the concentration of acid sites was slightly higher than in Al–Cu-3. More importantly, the selectivity to CO_2 was significantly enhanced over Al–Cu-5 indicating stronger deep oxidation capability as shown in Fig. 10b. In summary, the conversion on γ-Al_2O_3 and Al–Cu-3 was slightly higher than that on Al–Cu-5, but the latter exhibited higher activity in complete oxidation producing more CO_2. Besides the formation of noticeably larger amount of VC on Al–Cu-3 compared with Al–Cu-5 and Al–Cu-10, it formed other chlorinated byproducts as discussed earlier which resulted in less CO_2 compared with the other Al–Cu catalysts.

The Al–Cu-5 catalyst was selected for catalytic activity study at various reaction temperatures. Fig. 11a presents DCE conversion at temperatures between 250°C and 400°C over Al–Cu-5 and γ-Al_2O_3. Although the total conversion was higher on γ-alumina at low temperatures, it increased to 100% on

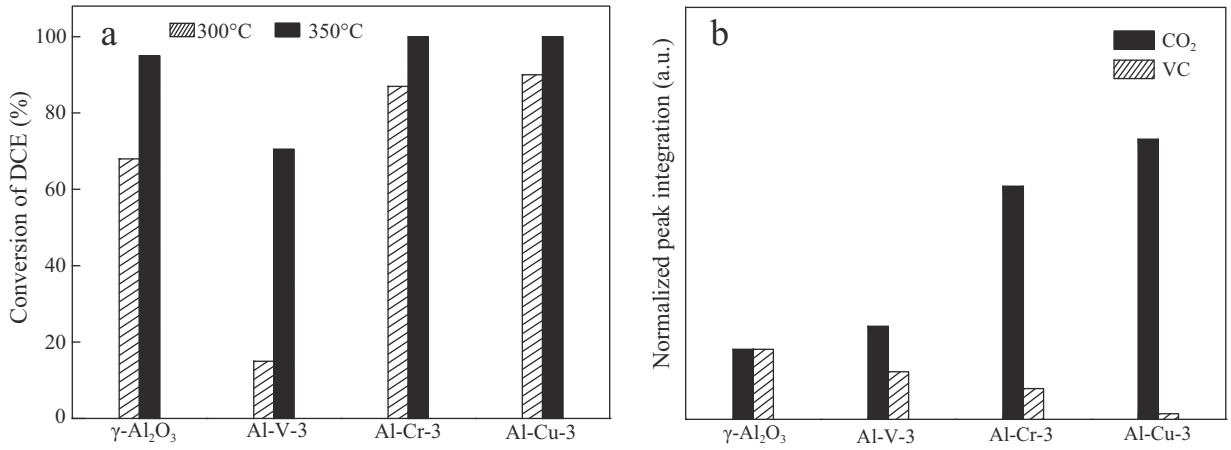

Fig. 9 – Conversion of DCE (a) and CO_2 and VC profiles after 5 hr on stream at 350°C (b) over undoped and doped γ-alumina containing 3% dopants. The peak areas of both products were normalized using the area of the same peaks in the γ-alumina spectrum as a reference for this figure.

both catalysts at 375°C. The capability for deep oxidation also varied noticeably with temperature for both catalysts. Fig. 11b presents the CO_2 profile over both catalysts represented by its normalized peak integration using its peak area in the spectrum from the reaction over γ-alumina at 250°C as a reference. While a negligible amount of CO_2 formed from the reaction over γ-alumina at 250°C, indicating week oxidation activity, noticeably larger amount formed over Al–Cu-5 at the same temperature indicating enhanced oxidation ability. The ability for deep oxidation increased slightly over γ-alumina with increasing the temperature, while it increased at a significantly higher rate over the doped catalyst. These results indicate that the surface of γ-alumina has a higher tendency towards adsorption and dehydrochlorination of DCE at lower temperatures. However, temperatures ≥375°C, increased the conversion to 100% and significantly enhanced the capability of the doped catalyst for deep oxidation. It is noteworthy to point out that the Cu-doped catalysts exhibited promising oxidation activity as compared to several reported catalysts, which have resulted in VC as a major product at temperatures as high as 450°C (López-Fonseca et al., 2000; Aranzabal et al., 2006; Huang et al., 2010; de Rivas et al., 2007).

Although it seems difficult to deduce a direct relationship between the catalytic activity and the measured number of acid sites, Table 2, it is evident that the higher surface acidity and the type as well as the concentration of metal dopant were decisive factors in the catalytic activity and product selectivity. This is evident from the noticeable decrease in the conversion over Al–Cu-10, Fig. 10b, which showed the lowest acid site concentration among the doped samples. In addition, the low activity of Al–V-3 may be correlated with its weaker acid sites as indicated by its lower temperature of ammonia desorption, Fig. 6, indicating that the stronger acid sites of the other catalysts may have played an important role in enhancing the catalytic activity.

The observed catalytic activities correlate with the H_2-TPR results indicating that the redox properties of the dopant ions played an important role in the observed activities. The

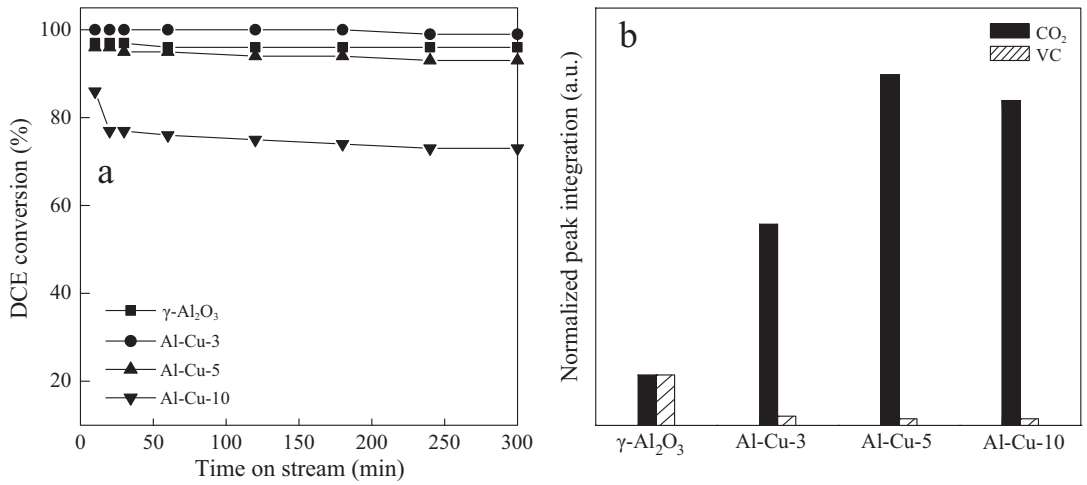

Fig. 10 – Conversion of DCE over Cu-doped γ-alumina *vs.* dopant concentration and time (a) and CO_2 and VC profiles *vs.* Cu^{2+} concentration after 5 hr (b) on stream at 350°C over Cu-doped catalysts.

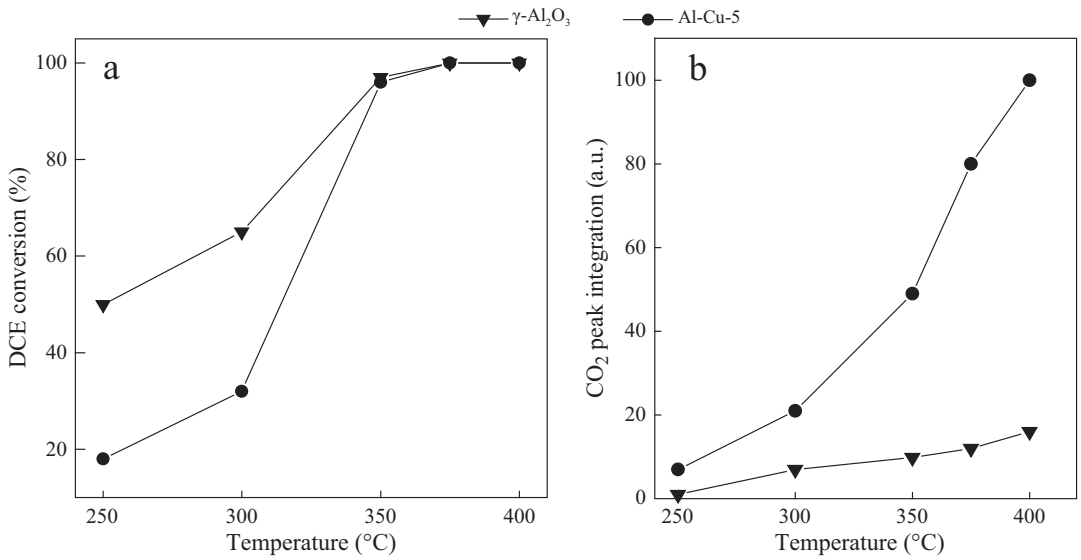

Fig. 11 – Conversion of DCE *vs.* reaction temperature after 5 hr on stream (a) and CO_2 profile represented by its normalized CO_2 peak integration after 5 hr (b) on stream over Al–Cu-5 and γ-Al_2O_3.

reduction profile of Al–V-3 which showed a peak at significantly higher temperature compared with the other catalysts correlates with its low catalytic activity. On the other hand, the higher reducibility of Al–Cu-5 explains its higher capability for complete oxidation compared with Al–Cu-3, which showed higher conversion but less complete oxidation. However, the high Cu^{2+} concentration in Al–Cu-10 resulted in an opposite effect, which may be referred to the possible presence of excess Cu^{2+} ions on the surface replacing the acidic Al^{3+} sites that are needed for the initial adsorption of DCE molecules as discussed below. These results and the fact that the observed textural properties showed no direct correlation with the catalytic activity, indicate that the key factors in determining the conversion as well as the deep oxidation capability are mainly the type as well as the concentration of the dopant ions.

2.3. DCE adsorption

The adsorption study of DCE on the surface of the catalysts at different temperatures provided some understanding of the possible steps involved in the reactions. Fig. 12 presents the FTIR spectra of species evolved on the surface of Al–Cu-3 at different temperatures after adsorption of DCE at 100°C. Adsorption on the other catalysts is compared and discussed below. The spectrum at 100°C seems complicated with broad unresolved bands in the region between 1700 and 3000 cm^{-1} indicating significant changes on the surface involving different intermediates. Most of these features started to disappear rapidly upon heating, which can be referred to decomposition and desorption. The peak at 725 cm^{-1} and the peaks between 2800 and 3000 cm^{-1} are due to ν_{C-Cl} and ν_{C-H} stretching vibrations, respectively. However, these peaks don't seem to refer to free DCE due to the absence of the ρCH_2 characteristic peak at 1230 cm^{-1}. This noticeable difference and their disappearance upon purging indicate that they refer to weakly adsorbed molecules. After purging at 100°C, the presence of different ν_{C-H} peaks in the region 2800–3100 cm^{-1} and the absence of peaks in the region <1000 cm^{-1}, where any absorption due to ν_{C-Cl} would appear, indicates the presence of adsorbed hydrocarbon intermediates containing no C–Cl bonds. The ν_{C-H} peaks decreased in intensity as the temperature was raised to 400°C indicating thermal decomposition and desorption.

In the ν_{O-H} region, two peaks appeared at 3780 and 3750 cm^{-1}, which can be referred to two types of terminal isolated OH groups, and a broad band centering around 3600 cm^{-1}, which can be referred to H-bonded or tri-bridged OH groups (Morterra and Magnacca, 1996). After purging, the peak at 3750 cm^{-1} disappeared and a new broad band appeared around 3400 cm^{-1} that can be referred to different types of

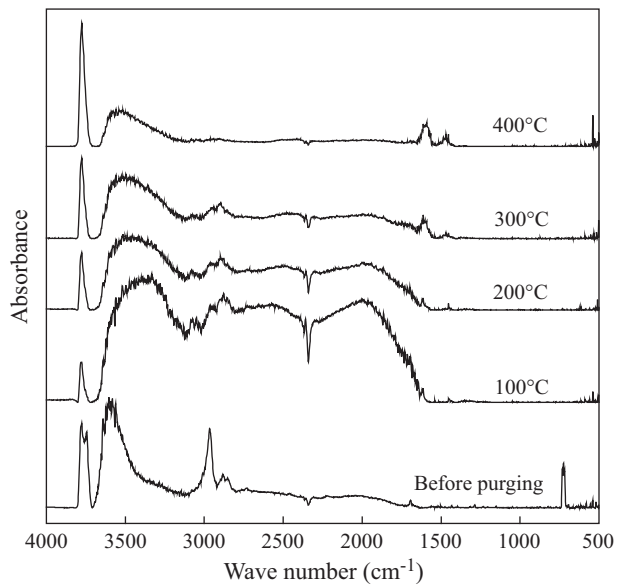

Fig. 12 – FTIR spectra of species on the surface of Al–Cu-3 at different temperatures after adsorption of DCE at 100°C.

H-bonded OH groups. This band decreased in intensity and shifted to higher frequency centering at 3550 cm^{-1} as the temperature was raised. The peak at 3780 cm^{-1} and the band at 3550 cm^{-1} were retained at 400°C indicating stable terminal isolated and H-bonded OH groups. These observations indicate that the initial adsorption of DCE involved interaction with oxygen sites and subsequent C–H bond activation forming OH intermediates. In a separate experiment, DCE was reintroduced at each temperature and the same results were obtained except that all peaks in the spectra (not shown) were more intense.

Interestingly, the different catalysts showed different modes of interaction with DCE as revealed by their FT-IR spectra after DCE adsorption. Fig. 13 displays the spectra of DCE adsorption/decomposition on the surface of Al–M-3 and γ-Al_2O_3 catalysts at temperatures between 100°C and 400°C. One noticeable feature is the strong peaks at 1612 and 1453 cm^{-1}, in the spectra of Al–Cr-3 which were very weak in the spectra of the other catalysts. These peaks increased in intensity as the temperature was raised above 100°C. The absence of ν_{C-Cl} absorption indicates that these peaks don't refer to adsorbed VC. In addition, these peaks were not associated with typical peaks that might represent C–H bonds of acetate or ethoxy species, such as the typical band due to deformation of CH_3 group below 1400 cm^{-1} (Rivas et al., 2007). Therefore, it is likely that these peaks refer to surface adsorbed C═C species bound to surface oxygen sites as shown in Fig. 14. The fact that the formation of such intermediate was enhanced at higher temperatures supports this suggestion since higher temperatures would enhance HCl and other adsorbed species removal allowing such intermediate to form and bind to the surface.

In the ν_{O-H} region, a broad band between 3200 and 3700 cm^{-1}, and a relatively sharp peak at 3780 cm^{-1} were observed in the spectra of all catalysts except Al–V-3 which showed complete absence of the peak at 3780 cm^{-1} at temperatures below 400°C and very weak features in the rest of the spectrum. The different catalysts showed different behaviors in their spectra upon heating. While γ-alumina showed a complete removal of the band centered around 3550 cm^{-1} at 400°C, Al–Cu-3 and Al–Cr-3 retained this band to a significant extent. On the other hand, the peak at 3780 cm^{-1},

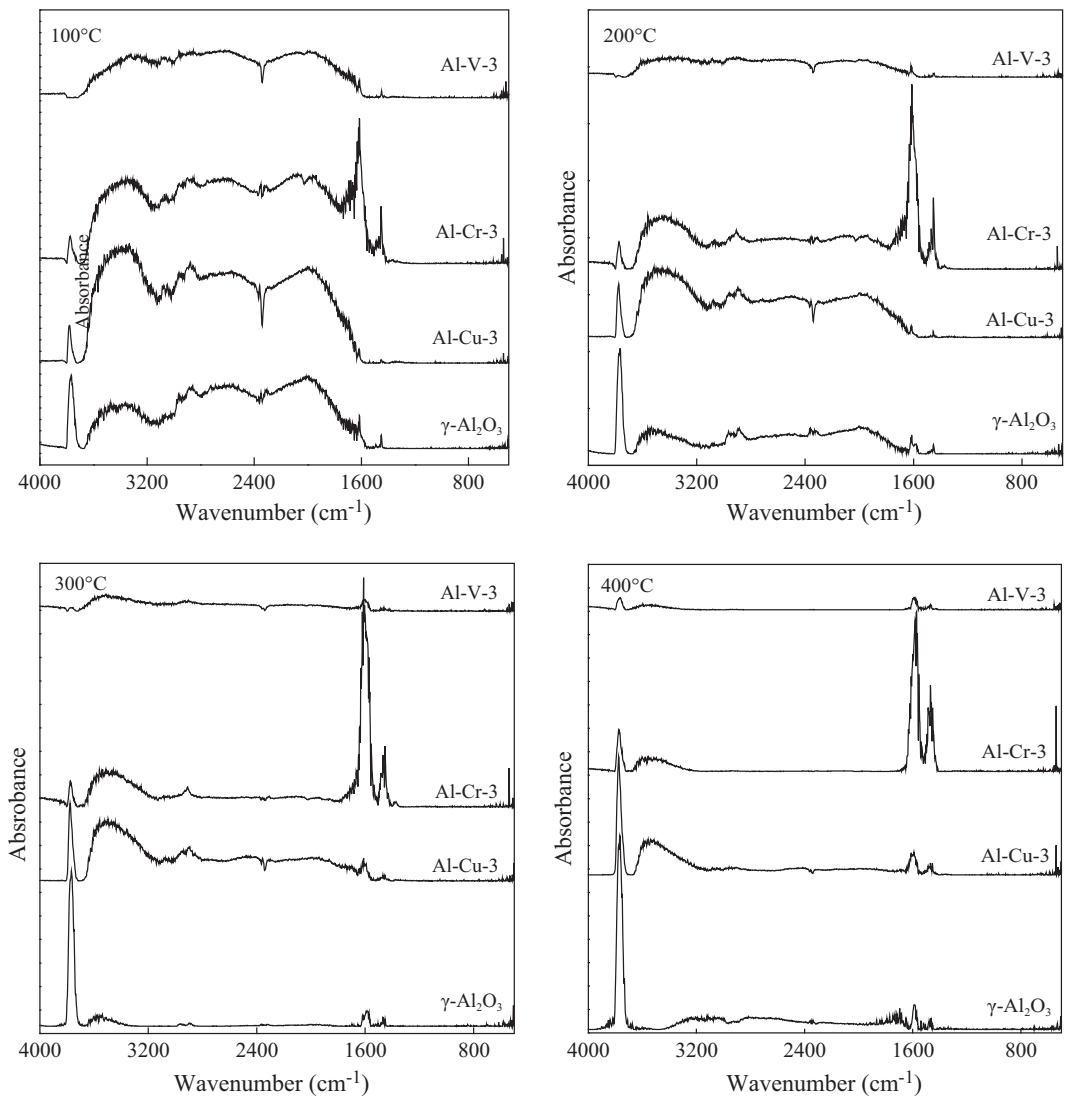

Fig. 13 – FT-IR spectra of species on the surface at temperatures between 100°C and 400°C after adsorption of DCE.

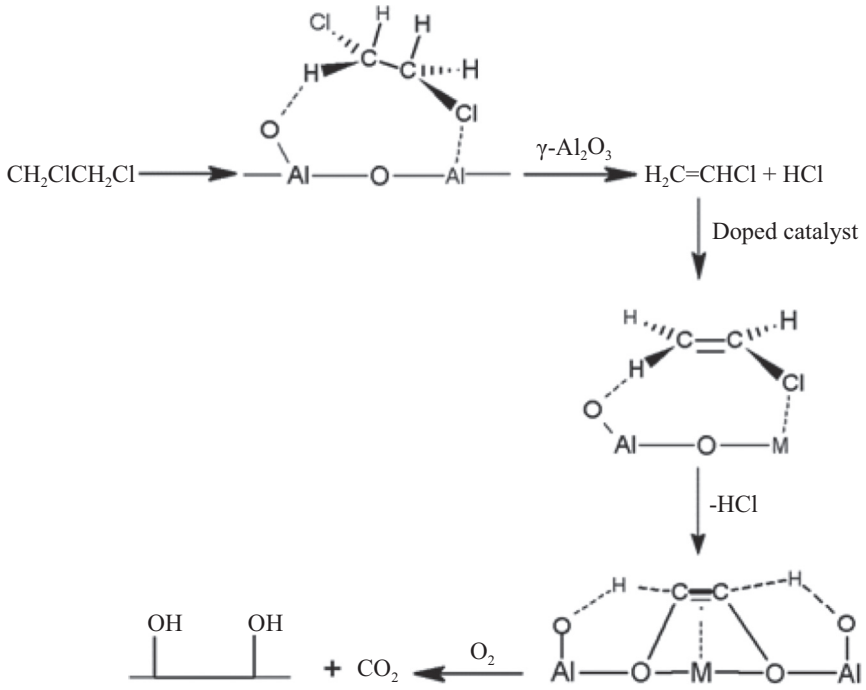

Fig. 14 – Suggested steps in the dehydrochlorination and oxidation of DCE. "M" refers to transition metal ions.

which was referred to terminal OH groups, showed a noticeable increase in intensity, especially on γ-alumina and Al–Cu-3, upon increasing the temperature.

The formation of different OH groups on the surface of the catalysts could be correlated with the observed catalytic activity. While, the more active catalysts showed significant formation of OH groups in the adsorption study, the least active catalyst, Al–V-3, showed minimum formation of these groups. Furthermore, the type of OH groups that formed may be correlated with the product selectivity. While the formation of terminal OH groups on γ-alumina was associated with hydrodechlorination only, the dominance of bridged OH groups on Al–Cu-3 and Al–Cr-3 was associated with enhanced deep oxidation. These observations may indicate that the OH groups that form on the surface from initial adsorption and decomposition of DCE play a role in promoting continuous reactions, as shown in Fig. 14, which presents proposed steps based on the known role of Lewis acid sites in dehydrochlorination and the current results of the FT-IR adsorption study.

Transition metal ions are known to promote redox reactions, and oxygen atoms bound to them in a mixed oxide lattice are usually more labile than those bound to aluminum ions. Therefore, the enhanced activity of the doped catalysts can be referred to combining the Lewis acidity of the alumina surface with the redox properties of the transition metal ions. It is also possible that transition metal ions play a role through abstraction and stabilization of the second chlorine atom promoting the cleavage of the second C–Cl bond, which is known for Cu-based catalysts. In addition, coordinatively unsaturated transition metal ions on the surface can also promote reactions through possible overlap between their occupied *d*-orbitals and antibonding π-molecular orbitals of adsorbed intermediates containing C═C. This type of interaction weakens the carbon-carbon bond facilitating its dissociation. This possible effect of the dopant ions may explain, in part, the observed catalytic oxidation activity trend, Al–Cu-3 > Al–Cr-3 > Al–V-3. This trend might be correlated with the back-bonding ability of the metal ions Cu^{2+}, Cr^{3+}, and V^{3+} with the *d*-configuration, d^9, d^3, and d^2, respectively. The different catalytic activities could be also, in part, referred to the ability of the doped ions to abstract and stabilize chlorine atoms. However, further work is still needed for better understanding of the different behavior of the ions in terms of stabilizing the observed intermediates, the type of OH groups, and the catalytic oxidation activity trend.

3. Conclusions

The employed sol–gel method resulted in mesoporous powders of undoped and metal-doped γ-alumina with high surface areas, large pore volumes, and significant acidity. The doped catalysts showed promising activity in the deep oxidation of 1,2-dichloroethane at relatively low temperatures compared with pure γ-alumina. Both types of catalysts, doped and undoped, exhibited 100% conversion in the temperature range of 350–400°C. The nature of the products was strongly dependent on the presence as well as on the type of dopant ion. Interestingly, Cu- and Cr-doped catalysts showed significantly higher catalytic activity in the deep oxidation of DCE. Retaining the γ-alumina acidity after doping combined with the oxidation-reduction capability of the transition metal ions played an important role in promoting dehydrodechlorination and further oxidation of the reaction intermediates. In addition, it was proposed that possible interaction between metal *d*-orbitals and π-molecular orbitals of C═C adsorbed species may have contributed to the enhanced deep oxidation of DCE. The results of this study show that catalysts based on

Cu-doped solid acids are promising for total oxidation of organic compounds.

Acknowledgment

The financial support from United Arab Emirates University through NRF grant, 2011, is acknowledged with gratitude.

REFERENCES

Aranzabal, A., González-Marcos, J.A., Ayastuy, J.L., González-Velasco, J.R., 2006. Kinetics of Pd/alumina catalysed 1,2-dichloroethane gas-phase oxidation. Chem. Eng. Sci. 61 (11), 3564–3576.

Chakraborty, B., Viswanathan, B., 1999. Surface acidity of MCM-41 by in situ IR studies of pyridine adsorption. Catal. Today 49 (1–3), 253–260.

de Rivas, B., López-Fonseca, R., González-Velasco, J.R., Gutiérrez-Ortiz, J.I., 2007. On the mechanism of the catalytic destruction of 1,2-dichloroethane over Ce/Zr mixed oxide catalysts. J. Mol. Catal. A Chem. 278 (1–2), 181–188.

de Rivas, B., Sampedro, C., Ramos-Fernández, E.V., López-Fonseca, R., Gascon, J., Makkee, M., et al., 2013. Influence of the synthesis route on the catalytic oxidation of 1,2-dichloroethane over CeO_2/H-ZSM5 catalysts. Appl. Catal. A Gen. 456, 96–104.

Gutiérrez-Alejandre, A., González-Cruz, M., Trombetta, M., Busca, G., Ramírez, J., 1998. Characterization of alumina–titania mixed oxide supports: part II: Al_2O_3-based supports. Microporous Mesoporous Mater. 23 (5–6), 265–275.

Huang, Q.Q., Xue, X.M., Zhou, R.X., 2010. Decomposition of 1,2-dichloroethane over CeO_2 modified USY zeolite catalysts: effect of acidity and redox property on the catalytic behavior. J. Hazard. Mater. 183 (1–3), 694–700.

Khaleel, A., 2006. Catalytic activity of mesoporous alumina for the hydrolysis and dechlorination of carbon tetrachloride. Micropor. Mesopor. Mater. 91 (1–3), 53–58.

Khaleel, A., Al-Mansouri, S., 2010. Meso-macroporous γ-alumina by template-free sol–gel synthesis: the effect of the solvent and acid catalyst on the microstructure and textural properties. Colloids Surf. A Physicochem. Eng. Asp. 369 (1–3), 272–280.

Khaleel, A., Al-Nayli, A., 2008. Supported and mixed oxide catalysts based on iron and titanium for the oxidative decomposition of chlorobenzene. Appl. Catal. B Environ. 80 (1–2), 176–184.

Khaleel, A., Dellinger, B., 2002. FT-IR investigation of adsorption and chemical decomposition of CCl_4 by high surface area aluminum oxide. Environ. Sci. Technol. 36 (7), 1620–1624.

Khaleel, A., Nawaz, M., Al-Hadrami, S., Greish, Y., Saeed, T., 2013. The effect of metal ion dopants (V^{3+}, Cr^{3+}, Fe^{3+}, Mn^{2+}, Ce^{3+}) and their concentration on the morphology and the texture of doped γ-alumina. Micropor. Mesopor. Mater. 168, 7–14.

Larrubia, M.A., Busca, G., 2002. An FT-IR study of the conversion of 2-chloropropane, o-dichlorobenzene and dibenzofuran on V_2O_5–MoO_3–TiO_2 SCR-DeNO_x catalysts. Appl. Catal. B Environ. 39 (4), 343–352.

Lif, J., Odenbrand, I., Skoglundh, M., 2007. Sintering of alumina-supported nickel particles under amination conditions: support effects. Appl. Catal. A Gen. 317 (1), 62–69.

López-Fonseca, R., Aranzabal, A., Steltenpohl, P., Gutiérrez-Ortiz, J.I., González-Velasco, J.R., 2000. Performance of zeolites and product selectivity in the gas-phase oxidation of 1,2-dichloroethane. Catal. Today 62 (4), 367–377.

Morterra, C., Magnacca, G., 1996. A case study: surface chemistry and surface structure of catalytic aluminas, as studied by vibrational spectroscopy of adsorbed species. Catal. Today 27 (3–4), 497–532.

Rivas, B., Rubén, L.-F., González-Velasco, J.R., Gutiérrez-Ortiz, J.I., 2007. On the mechanism of the catalytic destruction of 1,2-dichloroethane over Ce/Zr mixed oxide catalysts. J. Mole. Catal. A: Chem. 278, 181–188.

Scire, S., Minico, S., Crisafulli, C., 2003. Pt catalysts supported on H-type zeolites for the catalytic combustion of chlorobenzene. Appl. Catal. B Environ. 45 (2), 117–125.

Zhang, C.H., Wang, C., Zhan, W.C., Guo, Y.L., Guo, Y., Lu, G.Z., et al., 2013. Catalytic oxidation of vinyl chloride emission over $LaMnO_3$ and $LaB_{0.2}Mn_{0.8O3}$ (B = Co, Ni, Fe) catalysts. Appl. Catal. B Environ. 129, 509–516.

Editorial Board of Journal of Environmental Sciences

JOURNAL OF ENVIRONMENTAL SCIENCES

环境科学学报(英文版)

www.jesc.ac.cn

Aims and scope

Journal of Environmental Sciences is an international academic journal supervised by Research Center for Eco-Environmental Sciences, Chinese Academy of Sciences. The journal publishes original, peer-reviewed innovative research and valuable findings in environmental sciences. The types of articles published are research article, critical review, rapid communications, and special issues.

The scope of the journal embraces the treatment processes for natural groundwater, municipal, agricultural and industrial water and wastewaters; physical and chemical methods for limitation of pollutants emission into the atmospheric environment; chemical and biological and phytoremediation of contaminated soil; fate and transport of pollutants in environments; toxicological effects of terrorist chemical release on the natural environment and human health; development of environmental catalysts and materials.

For subscription to electronic edition

Elsevier is responsible for subscription of the journal. Please subscribe to the journal via http://www.elsevier.com/locate/jes.

For subscription to print edition

China: Please contact the customer service, Science Press, 16 Donghuangchenggen North Street, Beijing 100717, China. Tel: +86-10-64017032; E-mail: journal@mail.sciencep.com, or the local post office throughout China (domestic postcode: 2-580).

Outside China: Please order the journal from the Elsevier Customer Service Department at the Regional Sales Office nearest you.

Submission declaration

Submission of the work described has not been published previously (except in the form of an abstract or as part of a published lecture or academic thesis), that it is not under consideration for publication elsewhere. The publication should be approved by all authors and tacitly or explicitly by the responsible authorities where the work was carried out. If the manuscript accepted, it will not be published elsewhere in the same form, in English or in any other language, including electronically without the written consent of the copyright-holder.

Editorial

Authors should submit manuscript online at http://www.jesc.ac.cn. In case of queries, please contact editorial office, Tel: +86-10-62920553, E-mail: jesc@rcees.ac.cn. Instruction to authors is available at http://www.jesc.ac.cn.

Journal of Environmental Sciences (Established in 1989)
Volume 29 2015

Supervised by	Chinese Academy of Sciences	**Published by**	Science Press, Beijing, China
Sponsored by	Research Center for Eco-Environmental		Elsevier Limited, The Netherlands
	Sciences, Chinese Academy of Sciences	**Distributed by**	
Edited by	Editorial Office of Journal of	Domestic	Science Press, 16 Donghuangchenggen
	Environmental Sciences		North Street, Beijing 100717, China
	P. O. Box 2871, Beijing 100085, China		Local Post Offices through China
	Tel: 86-10-62920553; http://www.jesc.ac.cn	Foreign	Elsevier Limited
	E-mail: jesc@rcees.ac.cn		http://www.elsevier.com/locate/jes
Editor-in-chief	X. Chris Le	**Printed by**	Beijing Beilin Printing House, 100083, China

CN 11-2629/X **Domestic postcode: 2-580** **Domestic price per issue RMB ¥ 110.00**

ISSN 1001-0742